Journal of Marine Science and Technology

Volume 24 | Issue 5 Article 10

ANALYSIS OF WAVE INTERACTION WITH DOUBLE VERTICAL SLOTTED WALLS USING MBEM

Ching-Yun Yueh
Department of Harbor and River Engineering, National Taiwan Ocean University Keelung, Taiwan, R.O.C,
yuehcy@mail.ntou.edu.tw

Chih-Hao Su
Department of Harbor and River Engineering, National Taiwan Ocean University Keelung, Taiwan, R.O.C.

Chun-Chiang Wen
Department of Harbor and River Engineering, National Taiwan Ocean University Keelung, Taiwan, R.O.C

Shih-Hsuan Chuang
NCKU Hydraulic and Ocean Engineering R&D Foundation, Tainan, Taiwan, R.O.C.

Recommended Citation

Yueh, Ching-Yun; Su, Chih-Hao; Wen, Chun-Chiang; and Chuang, Shih-Hsuan (2016) "ANALYSIS OF WAVE INTERACTION WITH DOUBLE VERTICAL SLOTTED WALLS USING MBEM," *Journal of Marine Science and Technology*: Vol. 24: Iss. 5, Article 10.
DOI: 10.6119/JMST-016-0614-1
Available at: https://jmstt.ntou.edu.tw/journal/vol24/iss5/10

ANALYSIS OF WAVE INTERACTION WITH DOUBLE VERTICAL SLOTTED WALLS USING MBEM

Acknowledgements

The authors wish to express their gratitude for the financial aid from the Ministry of Science and Technology, Republic of China, and Project MOST No. 103-2221-E-019-065.

Journal of Marine Science and Technology, Vol. 24, No.5, pp. 992-1002 (2016)
DOI: 10.6119/JMST-016-0614-1

ANALYSIS OF WAVE INTERACTION WITH DOUBLE VERTICAL SLOTTED WALLS USING MBEM

Ching-Yun Yueh[1], Chih-Hao Su[1], Chun-Chiang Wen[1], and Shih-Hsuan Chuang[2]

Key words: coastal structures, permeable breakwater, slotted wall, multi-domain BEM, reflection, transmission.

ABSTRACT

In this paper, a multi-domain boundary element method (MBEM) is formulated and applied to study wave interaction with double vertical slotted walls, which are modeled as thin or non-thickness structures. Two-dimensional motion with wave crests parallel to the vertical slotted walls and linearized irrotational flow are assumed. The accuracy of the solution obtained using the numerical technique is demonstrated by comparing the numerical values with those obtained from experiments and from other analytical solutions. A comparison of the hydrodynamic performance of the breakwater with identical or different double vertical slotted walls is conducted. In addition, the numerical results of the wave reflection, transmission and energy dissipation for different relative permeable depths, chamber widths, and porosities are presented and discussed. Double vertical slotted walls with a longer rear wall are recommended because they more effectively suppressed wave energy at deeper submergence. The double vertical slotted walls also very effectively dissipate the incident wave energy. Our numerical results indicate that when the permeable middle part of the seaward (first) wall (dm_1/h = 0.6) and the permeable middle part of the leeward (second) wall (dm_2/h = 0.2) have different porosities of ε_1 = 0.5 and ε_2 = 0.3, respectively, the breakwater has a high reflection coefficient, a low transmission coefficient and the maximum energy dissipation coefficient. The maximum energy dissipation coefficient of 0.963 occurs at kh = 1.635.

I. INTRODUCTION

Various types of breakwaters are used throughout the world. The primary function of a breakwater is to protect the shoreward areas leeside of the structure by reducing the transmitted wave energy. An offshore breakwater, which is a type of permanent structure breakwater, may have some disadvantages, such as high construction costs, obstruction of water circulation and fish migration, and view obstruction, particularly in front of a pleasure beach or marina. Recently, vertical porous structures have become increasingly popular for protecting marinas and fishing harbors and for controlling shoreline erosion. The hydrodynamic efficiency of the porous structure is evaluated by testing the wave reflection, transmission and energy dissipation. Some examples of engineering applications of permeable breakwaters are located at Hanstholm (Denmark), Marsa el Brega (Libya), Osaka (Japan), Pass Christian Mississippi (USA) and Yeoho Port (Korea) (Ahmed and Schlenkhoff, 2014). Many experimental and theoretical studies were performed to determine the hydrodynamic efficiency of vertical submerged or emerged porous type structures. The simplest porous structure is a curtain-wall breakwater (CWB), which is often called a vertical barrier and consists of a comparatively thin concrete wall extending from above the water surface to some distance below the water surface. In deeper water waves (short waves), most of the wave energy is concentrated near the free surface, and a curtain-wall breakwater (CWB) that can effectively destroy or reflect this energy is therefore required. A single curtain-wall breakwater is capable of effectively reflecting the incident wave energy in deeper water (e.g., Dean, 1945; Ursell, 1947; Wiegel, 1960). A double curtain-wall breakwater is effective at reducing the reflection coefficient because waves reflecting off the front wall are out of phase with those reflecting off the rear wall (Liu and Li, 2010; Liu and Li, 2011). Curtain-wall-pile supported breakwaters (CPB), which have impermeable areas near the water surface, have been proposed to improve the performance of traditional curtain-wall breakwaters by permitting the exchange of the water across the breakwater. The CPB was proposed by Suh et al. (2006); they developed a mathematical model to predict the hydrodynamic characteristics of a CPB using an eigenfunction expansion method (EEM). Compared with conventional types of breakwaters, the CPB is environmentally friendly and eco-

Paper submitted 11/12/15; revised 03/08/16; accepted 06/14/16. Author for correspondence: Ching-Yun Yueh (e-mail: yuehcy@mail.ntou.edu.tw).
[1] Department of Harbor and River Engineering, National Taiwan Ocean University Keelung, Taiwan, R.O.C.
[2] NCKU Hydraulic and Ocean Engineering R&D Foundation, Tainan, Taiwan, R.O.C.

nomical for locations with poor soil conditions. Isaacson et al. (1998, 1999) developed a numerical model (EEM) of wave interaction with a partially submerged single barrier and a pair of thin vertical slotted barriers. Sundar and Subbarao (2002, 2003) performed a comprehensive experimental program to investigate the hydrodynamic pressures and forces on a quadrant front face pile-supported breakwater, which is expected to provide the combined benefits of both the semicircular and the pile breakwater. Ji and Suh (2010) showed that the hydrodynamic performance of a multiple-row CPB is improved compared with a single-row breakwater, whereas the difference between a double-row and triple-row breakwater is marginal. Recently, Laju et al. (2011) developed a numerical model for linear waves to investigate the coefficients of reflection, transmission, dimensionless run-up and dimensionless chamber oscillation characteristics of a single-row pile-supported skirt breakwater (PSSB) and a double-row PSSB. Later, Koraim and Salem (2012) conducted an experimental investigation on the hydrodynamic performance of a new of type of breakwater that consists of one row of half pipes suspended on supporting piles. Koraim et al. (2014) presented theoretical and experimental studies for the wave reflection, transmission and energy dissipation of the double rows of vertical piles formed by suspending horizontal steel C-shaped bars. Recent research by Ahmed and Schlenkhoff (2014) and Ahmed et al. (2014) investigated wave interaction with double vertical slotted walls using numerical simulations in a commercial CFD software (FLOW-3D), a physical model test and a semi-analytical model (eigenfunction expansion method, EEM). Their model consists of a pair of identical vertical slotted walls. Both walls have impermeable upper and lower parts and a permeable middle part with a porosity of 0.5. The draft of the upper and lower parts changed according to the permeable part (*dm*). Literature about the performance of double vertical slotted walls is rather scarce. The breakwater model considered here is similar to that of Ahmed and Schlenkhoff (2014). The main difference between Ahmed and Schlenkhoff (2014) and the present model is that in the former, the porosity and permeability draft of the middle part of the double slotted walls are identical, whereas in the present model, they are different. In the present study, to address the problem of wave interaction with a perforated breakwater, the method proposed by Sollitt and Cross (1972) and developed by Yu (1995) is adopted.

This article is organized as follows. In section 1, the primary objective of this study is presented along with the available literature reviews of experimental or theoretical studies. In section 2, the governing equation including all of the boundary conditions and the two-dimensional numerical model (MBEM) is formulated. In section 3, a limiting case of the current solution is discussed, and two verifying examples of the numerical method are provided. The numerical results of the wave reflection, transmission and energy loss coefficients of double vertical slotted walls for various types and wave conditions are presented and discussed. Finally, the main summary and conclusions of the numerical results in this paper are presented.

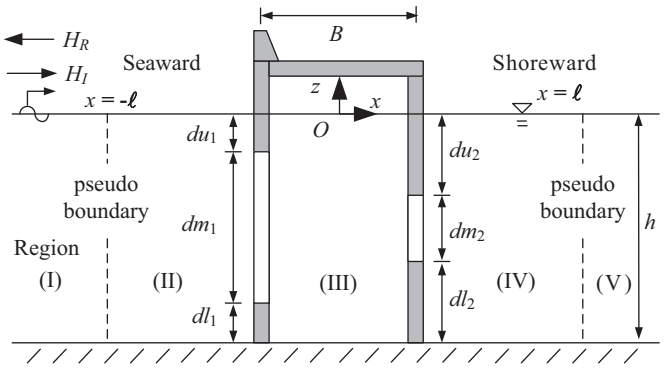

(a) Side view

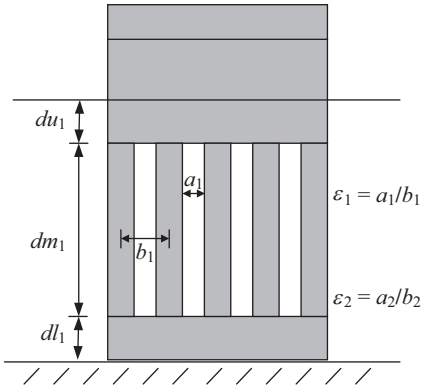

(b) Front view

Fig. 1. Definition sketch of breakwater with double vertical slotted walls.

THEORETICAL AND NUMERICAL CONSIDERATIONS

The definition of the two-dimensional problem is illustrated in Fig. 1. The model consists of a pair of vertical slotted walls. The first wall is located on the seaward side at distance (-*B*/2) from the origin point, and the second unit is located on the shoreward side at distance (*B*/2). Both walls have an impermeable upper and lower part and a permeable middle part. The submerged lengths of the two upper, middle and lower parts are denoted by du_1, du_2, dm_1, dm_2, dl_1 and dl_2, respectively. The subscripts 1 and 2 of *du*, *dm*, and *dl* indicate the submerged length of the first wall and the second wall, respectively. The distance between the centers of two neighboring slots is denoted as b_1 and b_2, and the widths of the openings are a_1 and a_2. Therefore, the porosities of the first and second walls are defined as $\varepsilon_1 = a_1/b_1$ and $\varepsilon_2 = a_2/b_2$, respectively. A Cartesian coordinate system (x-y plane with origin *O*) is used for the undisturbed free surface with the z-axis pointing vertically upward. The entire fluid domain is divided into five regions by a pseudo boundary at a distance $x = \pm\ell$: (I) the seaward region; (II) the region in front of the first wall; (III) the region between the vertical slotted walls; (IV) the region behind the second wall; and (V) the shoreward region.

1. Governing Equations

It is common to assume that the fluid outside and inside the permeable structure is inviscid and incompressible and that its motion is irrotational (Sollitt and Cross, 1972). We can then define the velocity potential $\Phi^j(x, z; t)$ that satisfies the Laplace equation:

$$\nabla^2\Phi^j(x, z; t) = \frac{\partial^2\Phi^j}{\partial x^2} + \frac{\partial^2\Phi^j}{\partial z^2} = 0,\ j = \mathrm{I} \sim \mathrm{V} \tag{1}$$

The incident wave is specified to propagate in the positive x-direction with an amplitude ζ_0 and an angular frequency σ. The velocity potential $\Phi^j(x, z; t)$ of the linearized wave motion can be expressed as:

$$\Phi^j(x, z; t) = \frac{g\zeta_0}{\sigma}\phi^j(x, z)\cdot\exp(-i\sigma t),\ j = \mathrm{I} \sim \mathrm{V} \tag{2}$$

where $i = \sqrt{-1}$, g = gravitational constant, and ϕ^j = spatial velocity potential satisfying the Laplace equation: $\nabla^2\phi^j(x, z) = 0$.

2. Boundary Conditions

Assuming a constant air pressure, the linearized boundary condition on the free surface can be obtained from the kinematic and dynamic boundary conditions:

$$\frac{\partial\phi^j}{\partial z} = \frac{\sigma^2}{g}\phi^j \text{ on } z = 0,\ j = \mathrm{I} \sim \mathrm{V} \tag{3}$$

The boundary conditions on the impermeable sea bed and vertical slotted walls are given by:

$$\frac{\partial\phi^j}{\partial z} = 0 \text{ on } z = -h,\ j = \mathrm{I} \sim \mathrm{V} \tag{4}$$

$$\frac{\partial\phi^j}{\partial x} = 0 \quad \text{on } x = -B/2, \text{ for } -du_1 \le z \le 0, \text{ and } -h \le z \le -(du_1 + dm_1)\ j = \mathrm{II}, \mathrm{III} \tag{5}$$

$$\frac{\partial\phi^j}{\partial x} = 0, \text{ on } x = B/2, \text{ for } -du_2 \le z \le 0 \text{ and } -h \le z \le -(du_2 + dm_2)\ j = \mathrm{III}, \mathrm{IV} \tag{6}$$

3. Matching Conditions

Assuming that the vertical slotted wall is a rigid homogeneous porous medium, the condition on the vertical slotted wall is given by:

$$\frac{\partial\phi^{\mathrm{II}}}{\partial x} = -\frac{\partial\phi^{\mathrm{III}}}{\partial x} = ikG\left(\phi^{\mathrm{II}} - \phi^{\mathrm{III}}\right) \text{ on } x = -B/2 \text{ for } -(du_1 + dm_1) \le z \le -du_1 \tag{7}$$

$$\frac{\partial\phi^{\mathrm{III}}}{\partial x} = -\frac{\partial\phi^{\mathrm{IV}}}{\partial x} = ikG\left(\phi^{\mathrm{III}} - \phi^{\mathrm{IV}}\right) \text{ on } x = B/2 \text{ for } -(du_2 + dm_2) \le z \le -du_2 \tag{8}$$

where G is the porous effect parameter (Yu, 1995), and k = wave number satisfying the dispersion relation.

$$\sigma^2 = gk \tanh kh$$

The complex porous effect parameter G can be estimated using $G = \dfrac{\varepsilon}{kb(f - is)}$, where ε, f, s, and b are the porosity, the linearized resistance coefficient, the inertial coefficient, and the thickness of the porous plate, respectively. The resistance effect causes wave energy dissipation, and the inertial effect produces the phase shift of the wave motion. When $|G|$ equals zero, the perforated barrier simplifies to an impermeable barrier; when $|G|$ tends to infinity, the barrier becomes entirely transparent.

Both energy and mass fluxes through the pseudo boundary must be conserved:

$$\phi^{\mathrm{I}} = \phi^{\mathrm{II}} \text{ on } x = -\ell \tag{9}$$

$$\frac{\partial\phi^{\mathrm{I}}}{\partial x} = \frac{\partial\phi^{\mathrm{II}}}{\partial x} \text{ on } x = -\ell \tag{10}$$

$$\phi^{\mathrm{IV}} = \phi^{\mathrm{V}} \text{ on } x = \ell \tag{11}$$

$$\frac{\partial\phi^{\mathrm{IV}}}{\partial x} = \frac{\partial\phi^{\mathrm{V}}}{\partial x} \text{ on } x = \ell \tag{12}$$

Because the pseudo boundary at $x = -\ell, \ell$ is sufficiently far from the vertical slotted walls, the evanescent waves induced by the existence of vertical slotted walls are sufficiently damped to disappear in region (I) and region (V). The spatial velocity potential $\phi^{\mathrm{I}}(x, z)$ in region (I) with a constant water depth h can then be expressed as follows:

$$\phi^{\mathrm{I}}(x, z) = \left[\exp\left(ik(x + \ell)\right) + R\cdot\exp\left(-ik(x + \ell)\right)\right]\frac{\cosh k(h + z)}{\cosh kh} \tag{13}$$

where R is the complex reflection coefficient.

At the pseudo boundary ($x = -\ell$), the spatial velocity potential and its normal derivative in the negative x-direction

are given by:

$$\phi^{\mathrm{I}} = (1+R)\frac{\cosh k(h+z)}{\cosh kh} \text{ on } x=-\ell \tag{14}$$

and

$$\frac{\partial\phi^{\mathrm{I}}}{\partial x} = ik(1-R)\frac{\cosh k(h+z)}{\cosh kh} \text{ on } x=-\ell \tag{15}$$

respectively.

The spatial velocity potential $\phi^{\mathrm{V}}(x,z)$ in region (V) with a constant water depth h can then be expressed as follows:

$$\phi^{\mathrm{V}}(x,z) = Te^{ik(x-\ell)}\frac{\cosh k(h+z)}{\cosh kh} \tag{16}$$

where T is the complex transmission coefficient.

At the pseudo boundary ($x=\ell$), the spatial velocity potential and its normal derivative in the negative x-direction are given by:

$$\phi^{\mathrm{V}} = T\frac{\cosh k(h+z)}{\cosh kh} \text{ on } x=\ell \tag{17}$$

and

$$\frac{\partial\phi^{\mathrm{V}}}{\partial x} = ikT\frac{\cosh k(h+z)}{\cosh kh} \text{ on } x=\ell \tag{18}$$

respectively.

By substituting Eq. (14) into Eq. (9), multiplying both sides by $\cosh k(h+z)$, and integrating from $-h$ to 0, the reflection coefficient is expressed as:

$$R = -1+\frac{k}{N_0\sinh kh}\int_{-h}^{0}\phi^{\mathrm{II}}\cosh k(h+z)dz \text{ on } x=-\ell \tag{19}$$

where $N_0 = \frac{1}{2}(1+2kh/\sinh 2kh)$.

By substituting Eq. (16) into Eq. (11), multiplying both sides by $\cosh k(h+z)$, and integrating from $-h$ to 0, the transmission coefficient is expressed as:

$$T = \frac{k}{N_0\sinh kh}\int_{-h}^{0}\phi^{\mathrm{IV}}\cosh k(h+z)dz \text{ on } x=\ell \tag{20}$$

4. Numerical Method

According to Green's second identity, the spatial velocity potentials in regions (II), (III) and (IV) can be written as follows:

$$2\pi\phi^{j}(x,z) = \int_{\Gamma}\left[\phi^{j}(\xi,\eta)\frac{\partial(\ln r)}{\partial n} - (\ln r)\frac{\partial\phi^{j}(\xi,\eta)}{\partial n}\right]ds, \quad j=\mathrm{II}\sim\mathrm{IV} \tag{21}$$

where Γ is the boundary in region (j), (ξ, η) are the coordinates of a point on boundary Γ, $r=\sqrt{(x-\xi)^2+(z-\eta)^2}$, and n is the unit normal vector on boundary Γ pointing outward.

We can now derive the integral representation of ϕ^j for points $P_B(\xi',\eta')$ lying on boundary Γ when the boundary is smooth. The boundary integral equation can be expressed as:

$$\pi\phi^{j}(\xi',\eta') = \int_{\Gamma}\left[\phi^{j}(\xi,\eta)\frac{\partial(\ln r')}{\partial n} - (\ln r')\frac{\partial\phi^{j}(\xi,\eta)}{\partial n}\right]ds, \quad j=\mathrm{II}\sim\mathrm{V} \tag{22}$$

where $r'=\sqrt{(\xi'-\xi)^2+(\eta'-\eta)^2}$.

The boundary Γ in Eq. (22) is discretized into N^j constant elements, where N^j is the number of constant elements in region (j). The values of the boundary quantity ϕ^j and its normal derivative $\partial\phi^j/\partial n$ are assumed to be constant over each element and equal to their given value at the mid-point of the element. The discretized form of Eq. (22) can be applied consecutively for all the nodes, yielding a system of N^j linear algebraic equations that are arranged in matrix form:

$$\left[\bar{U}^{j}\right]\left\{\phi^{j}\right\} = \left[U^{j}\right]\left\{\frac{\partial\phi^{j}}{\partial n}\right\}, \quad j=\mathrm{II}\sim\mathrm{IV} \tag{23}$$

where

$$\bar{U}^{j}_{\alpha\beta} = \int_{\Gamma_\beta}\frac{\partial(\ln r')}{\partial n}ds_\beta - \pi\delta_{\alpha\beta}, \quad j=\mathrm{II}\sim\mathrm{IV} \tag{24}$$

$$U^{j}_{\alpha\beta} = \int_{\Gamma_\beta}(\ln r')ds_\beta, \quad j=\mathrm{II}\sim\mathrm{IV} \tag{25}$$

where $\delta_{\alpha\beta}$ is the Kronecker delta, which is defined as $\delta_{\alpha\beta}=0$ for $\alpha\neq\beta$ and $\delta_{\alpha\beta}=1$ for $\alpha=\beta$.

We can now rewrite Eq. (23) in another matrix form:

$$\begin{bmatrix}\left[\bar{U}^{\mathrm{II}}\right] & 0 & 0\\ 0 & \left[\bar{U}^{\mathrm{III}}\right] & 0\\ 0 & 0 & \left[\bar{U}^{\mathrm{IV}}\right]\end{bmatrix}\begin{Bmatrix}\{\phi^{\mathrm{II}}\}\\ \{\phi^{\mathrm{III}}\}\\ \{\phi^{\mathrm{IV}}\}\end{Bmatrix} = \begin{bmatrix}\left[U^{\mathrm{II}}\right] & 0 & 0\\ 0 & \left[U^{\mathrm{III}}\right] & 0\\ 0 & 0 & \left[U^{\mathrm{IV}}\right]\end{bmatrix}\begin{Bmatrix}\left\{\frac{\partial\phi^{\mathrm{II}}}{\partial n}\right\}\\ \left\{\frac{\partial\phi^{\mathrm{III}}}{\partial n}\right\}\\ \left\{\frac{\partial\phi^{\mathrm{IV}}}{\partial n}\right\}\end{Bmatrix} \tag{26}$$

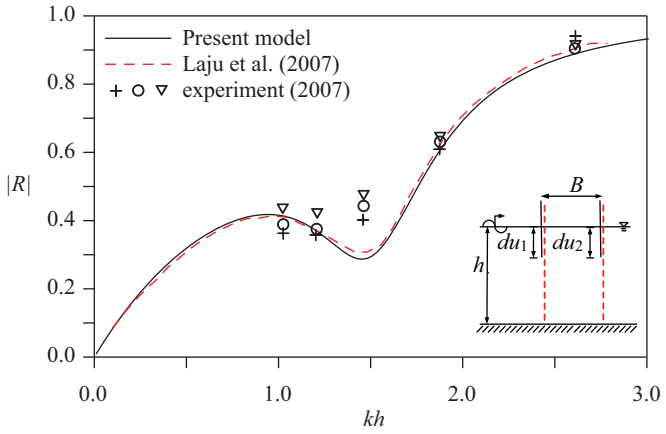

(a) Reflection coefficient $|R|$

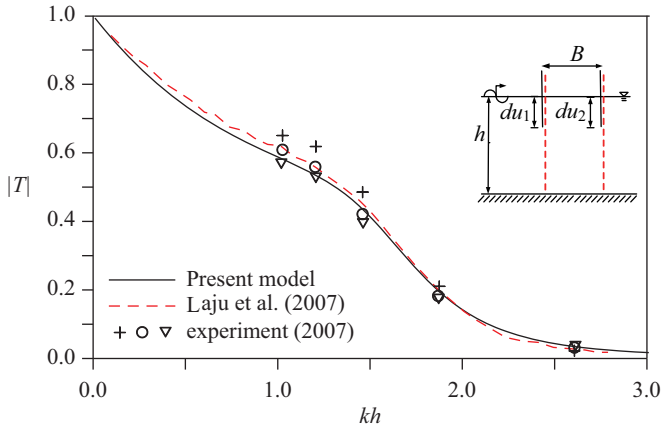

(b) Transmission coefficient $|T|$

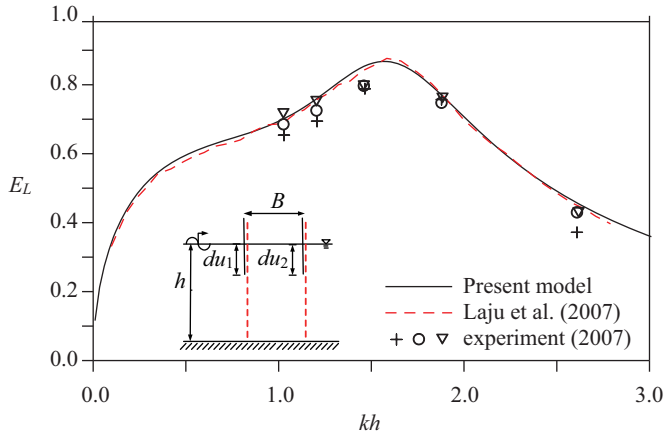

(c) Energy dissipation coefficient E_L

Fig. 2. Comparison between the present solution and that of Laju et al. (2007) as a function of kh for s = 1.0, f = 2.0, $\varepsilon_1 = \varepsilon_2$ = 0.25, B/h = 0.5 and $du_1/h = du_2/h$ = 0.35.

By substituting Eqs. (3)-(8) into Eq. (26), the solutions of the spatial velocity potential on each boundary can be obtained. The reflection coefficient R and transmission coefficient T can also be calculated using Eq. (19) and Eq. (20). From considerations of energy conservation, R and T are related to the energy dissipation coefficient E_L:

$$E_L = 1 - |R|^2 - |T|^2 \tag{27}$$

III. NUMERICAL RESULTS AND DISCUSSION

1. Verifying Examples of the Numerical Method

The multi-domain boundary element method (MBEM) was formulated as described in Sec. 2 and applied to study the hydrodynamic performance of wave interaction with double vertical slotted walls, which are modeled as thin or non-thickness structures in normal incident waves. To examine the reliability and the accuracy of the numerical method adopted here, two case studies are presented and discussed in this section. The accuracy of the solution is demonstrated by comparing the numerical values with those obtained from experiments and from other analytical solutions. In the first verifying example, we consider the case with two closely spaced rows of a pile-supported impermeable skirt breakwater. The numerical results are shown in Fig. 2 as continuous lines; the dashed lines and the marks indicate the numerical solution and experimental data obtained by Laju et al. (2007), respectively. This figure shows the variation of the reflection, transmission and energy dissipation coefficients as a function of the dimensionless wave number kh due to a constant chamber width (B/h = 0.5), an equal porosity ($\varepsilon_1 = \varepsilon_2$ = 0.25) and an equal submergence depth ($du_1/h = du_2/h$ = 0.35). For extremely long incident waves ($kh \to 0$), the reflection and transmission coefficient tend to approach zero and unity, respectively. In this case, the pile-supported skirt breakwater is ineffective. These figures show that our numerical results are in reasonably good agreement with the solutions obtained by the previous researchers.

The second verifying example uses a pair of identical vertical slotted walls with impermeable upper and lower parts and permeable middle parts with equal porosities of $\varepsilon_1 = \varepsilon_2$ = 0.5. The reflection, transmission and energy dissipation coefficients are plotted against kh for B/h = 0.5 in Fig. 3. In this figure, the dashed lines and the symbols represent the Ahmed and Schlenkhoff (2014) analytical solution and experimental results, respectively. The present results (solid lines) follow the estimated curves obtained by Ahmed and Schlenkhoff (2014) fairly well. In this figure, as kh increases, the wave reflection coefficient increases, and the transmission coefficient decreases. The maximum energy dissipation coefficient occurs at approximately E_L = 0.8 at kh = 2.0, $dm_1/h = dm_2/h$ = 0.6. However, the previous studies primarily included double vertical slotted walls with identical permeable depth and porosity. Therefore, the effect of unequal submerged permeable depth or porosity are considered in the present study to discover different breakwater types that are capable of dissipating a huge portion of the wave energy.

2. Influence of the Relative Permeable Depth (dm/h)

The influence of the permeable middle parts "dm_1" and "dm_2"

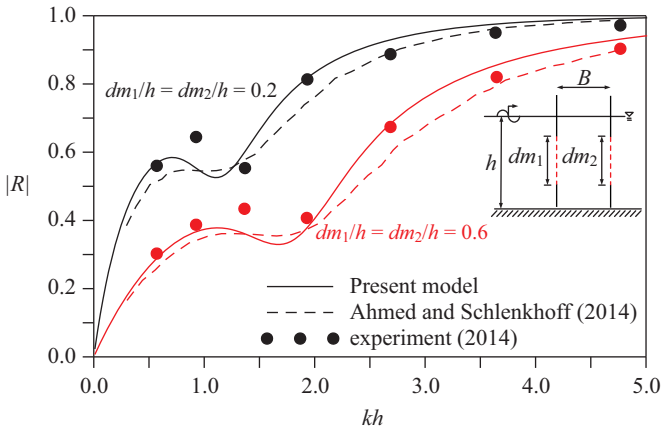

(a) Reflection coefficient $|R|$

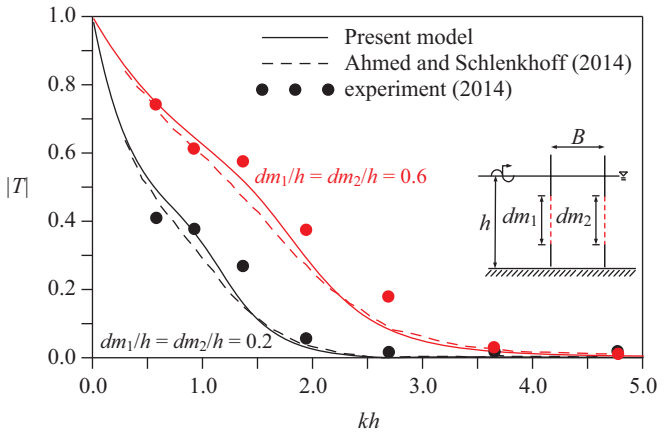

(b) Transmission coefficient $|T|$

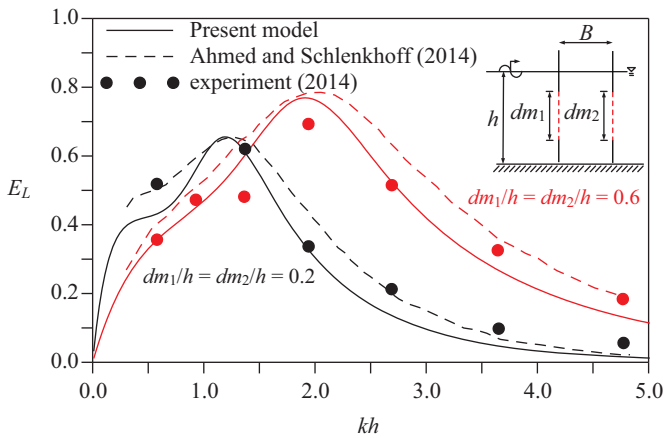

(c) Energy dissipation coefficient E_L

Fig. 3. Comparison of present model with the experimental and semi-analytical results of Ahmed and Schlenkhoff (2014) as a function of *kh* for $s = 1.0$, $f = 2.0$, $B/h = 0.5$ and $\varepsilon_1 = \varepsilon_2 = 0.5$.

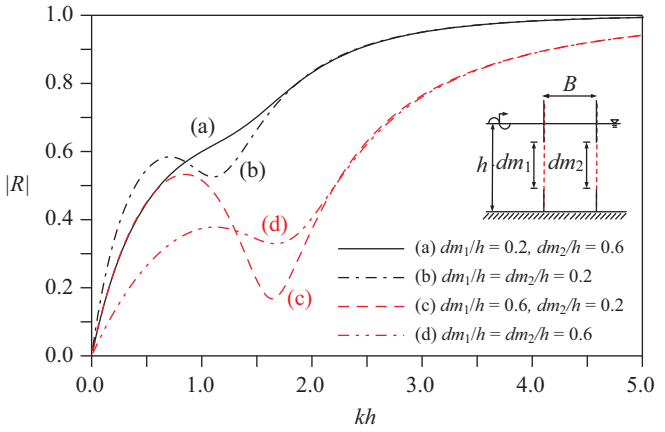

(a) Reflection coefficient $|R|$

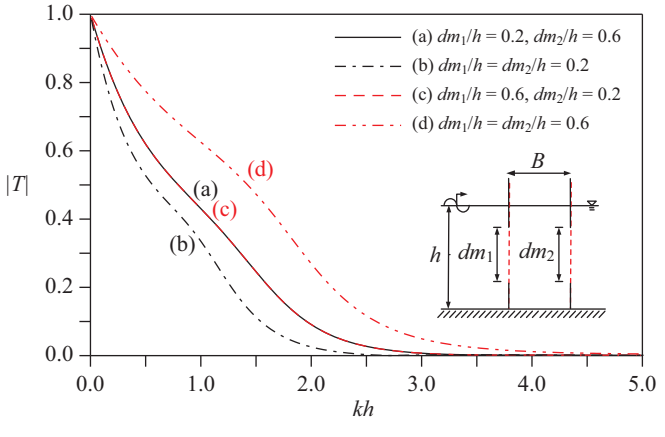

(b) Transmission coefficient $|T|$

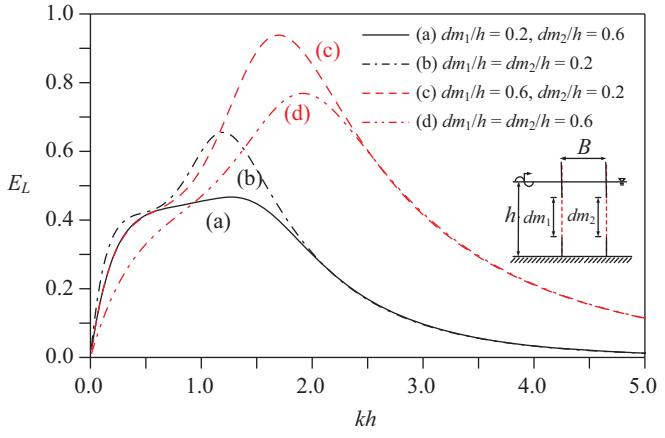

(c) Energy dissipation coefficient E_L

Fig. 4. Influence of the different relative permeable depths as a function of *kh* for $B/h = 0.5$ and $\varepsilon_1 = \varepsilon_2 = 0.5$.

at identical or unequal submerged depths on the hydrodynamic characteristics of double vertical slotted walls is plotted in Fig. 4, which indicate the reflection, transmission and energy dissipation coefficients as a function of *kh*. The upper and lower parts are impermeable; four cases of various relative permeability draft were examined at the following water depths: case (a) $dm_1/h = 0.2$, $dm_2/h = 0.6$, case (b) $dm_1/h = dm_2/h = 0.2$, case (c) $dm_1/h = 0.6$, $dm_2/h = 0.2$, and case (d) $dm_1/h = dm_2/h = 0.6$. For cases (b) and (d), the permeable depths are identical and match the results of Ahmed and Schlenkhoff (2014).

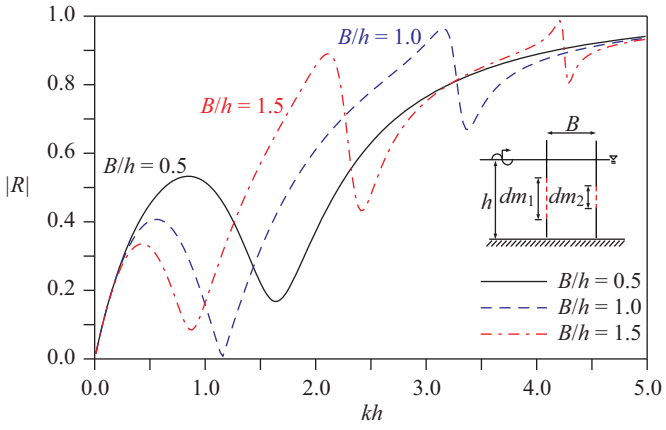

(a) Reflection coefficient $|R|$

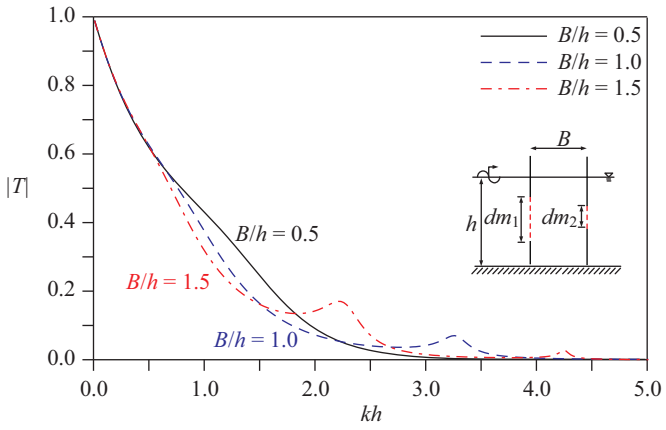

(b) Transmission coefficient $|T|$

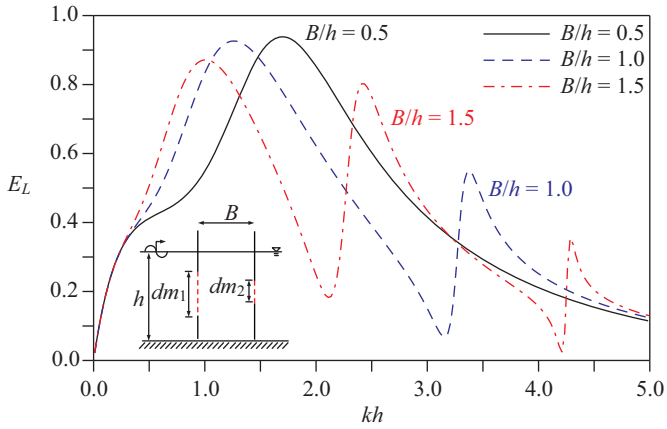

(c) Energy dissipation coefficient E_L

Fig. 5. Effect of the different relative chamber widths on $|R|$, $|T|$ and E_L as a function of kh for $dm_1/h = 0.6$, $dm_2/h = 0.2$ and $\varepsilon_1 = \varepsilon_2 = 0.5$.

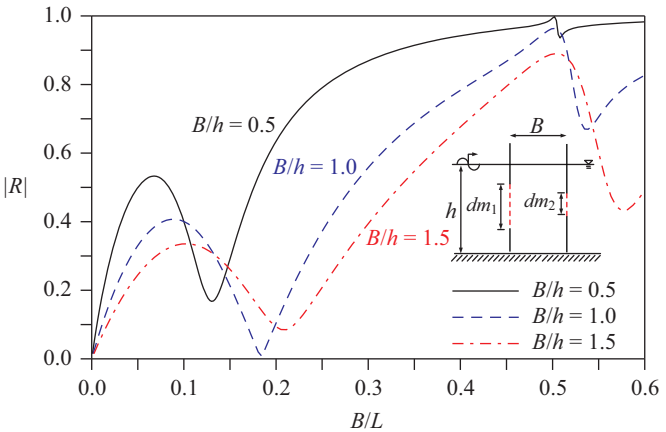

(a) Reflection coefficient $|R|$

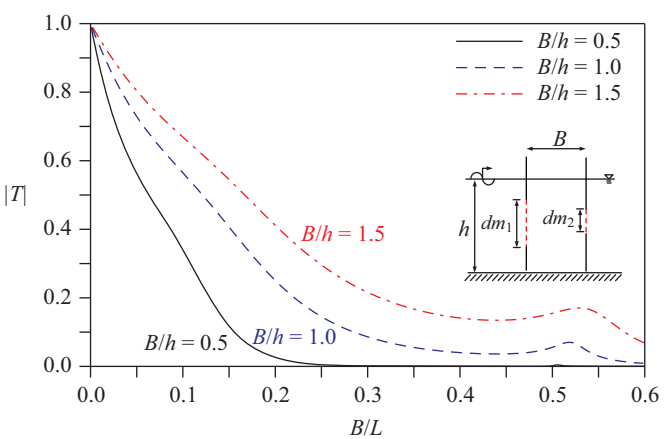

(b) Transmission coefficient $|T|$

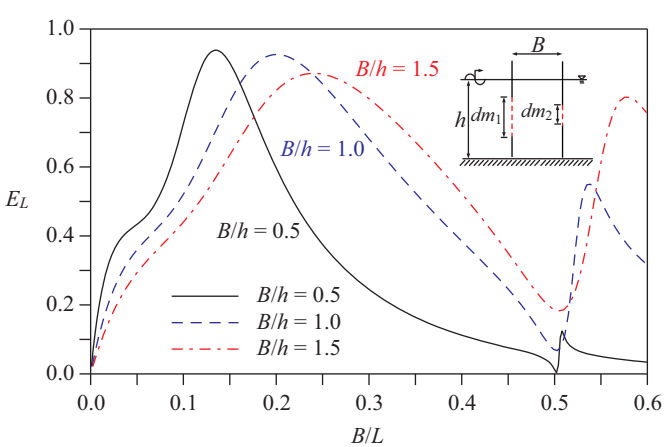

(c) Energy dissipation coefficient E_L

Fig. 6. Effect of the different relative chamber widths on $|R|$, $|T|$ and E_L as function of B/L for $dm_1/h = 0.6$, $dm_2/h = 0.2$ and $\varepsilon_1 = \varepsilon_2 = 0.5$.

Cases (a) and (c) are our numerical solutions for comparison. Fig. 4 shows a comparison of the reflection, transmission and energy dissipation coefficients of double vertical slotted walls as a function of kh for $dm_1/h = 0.2$ and 0.6 and $dm_2/h = 0.2$ and 0.6.

As intuitively expected, the reflection coefficient decreases as the relative middle permeable part of the seaward wall (dm_1/h) increases, and the transmission coefficient increases with increasing dm_1/h. The figures also show that for the cases of (b) and (d), the reflection coefficient $|R|$ increases with increasing kh at fixed $dm_1/h = dm_2/h$ and increases with decreas-

ing $dm_1/h = dm_2/h$. The transmission coefficient $|T|$ follows the opposite trend. A maximum energy dissipation coefficient of 0.8 is found for the identical relative permeable part (case (d) $dm_1/h = dm_2/h = 0.6$), especially for an intermediate water depth. It is crucial to compare the influence of the two identical permeable parts of the double vertical slotted walls with the influence of unequal permeable parts. When the relative chamber width is fixed ($B/h = 0.5$), the middle part of the slotted wall is permeable with a porosity of $\varepsilon_1 = \varepsilon_2 = 0.5$. From our numerical results in case (c), the middle permeable part of the seaward (first) wall ($dm_1/h = 0.6$) and the middle permeable part of the leeward (second) wall ($dm_2/h = 0.2$) have the same porosity of $\varepsilon_1 = \varepsilon_2 = 0.5$, which shows that the maximum energy dissipation coefficient of 0.938 occurs at $kh = 1.685$. While there is no significant difference in the high-frequency region ($kh > 2.0$), the performance of the double vertical slotted walls at $1.0 < kh < 2.0$ is greatly improved in case (c) ($dm_1/h = 0.6$ and $dm_2/h = 0.2$).

3. Influence of the Relative Chamber Width (B/h)

The relative chamber width (B/h) varies as a proportion of the water depth, and $B/h = 0.5$, 1.0 and 1.5 were studied in this research. The effect of B/h on the reflection, transmission and energy dissipation coefficients as a function of kh is shown in Fig. 5, where both middle parts are permeable ($\varepsilon_1 = \varepsilon_2 = 0.5$) but the submerged depths differ ($dm_1/h = 0.6$ and $dm_2/h = 0.2$). This figure shows that as B/h increases, the oscillation of $|R|$ and $|T|$ and the E_L coefficient increase; this figure also shows peaks in $|R|$, $|T|$ and the E_L coefficient.

The number of peaks increases with increasing relative chamber width. For short waves or a large dimensionless wavenumber (kh), most of the kinetic energy is concentrated closer to the still water level, and a large amount of wave energy is reflected by the impermeable upper part. Therefore, the transmission coefficient is very small. Fig. 5(c) shows that the energy dissipation coefficients E_L for double slotted walls reach their respective maximums of more than 0.8 at kh = 0.5~2.0 depending on the relative chamber width and then rapidly decrease as kh continues to increase. Changing the x-axis of Fig. 5, which is kh, to B/L, Fig. 6 shows the variation of the $|R|$, $|T|$ and E_L coefficient versus B/L (L: wavelength) for different spacings of the relative chambers. The variation of $|R|$, $|T|$ and the E_L coefficients in Fig. 6 are more regular than those in Fig. 5. For a fixed B/L, the total wave energy dissipation can be maximized; therefore, the reflection coefficient can be minimized, as shown in Fig. 6.

Regardless of the variation in the relative chamber width, the maximum reflection coefficient occurs when the ratio of the chamber width (B) to the wavelength (L) at $B/L \approx 0.5$ is associated with the minimum value of E_L. For the case of double slotted walls, the second wall should not be constructed at a distance where the wavelength of the incident wave is twice the chamber width; the energy dissipation coefficient has minimum values at $B/L \approx 0.5$.To find the best design of a double vertical slotted wall breakwater with the optimal values of porosity (ε_1, ε_2) and middle permeable part (dm_1/h,

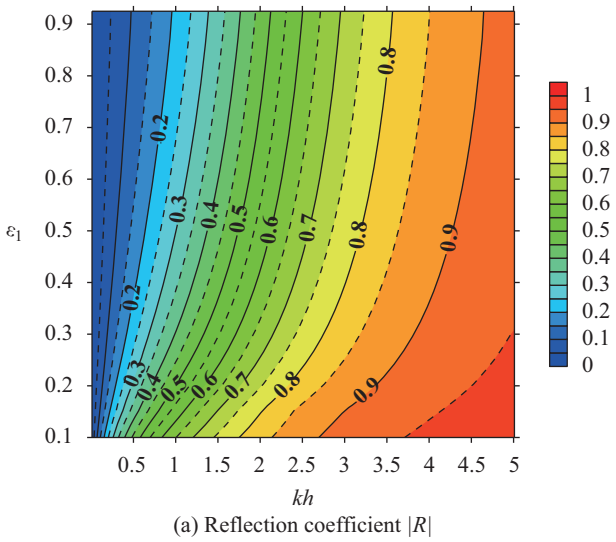

(a) Reflection coefficient $|R|$

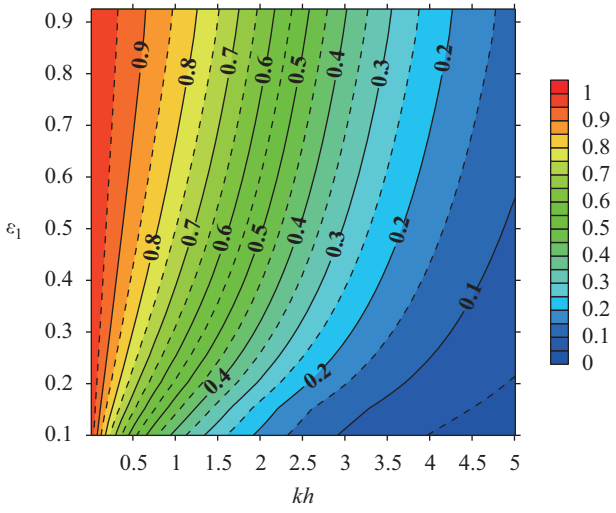

(b) Transmission coefficient $|T|$

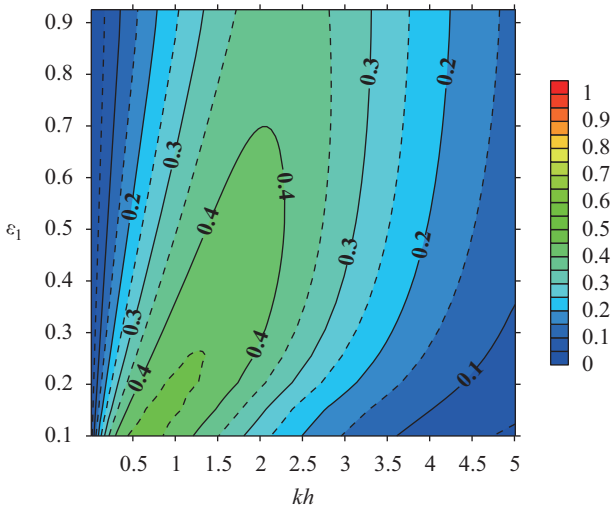

(c) Energy dissipation coefficient E_L

Fig. 7. Contour plots of $|R|$, $|T|$ and E_L coefficients as a function of kh and porosity ε_1 for single slotted wall at $dm_1/h = 0.6$.

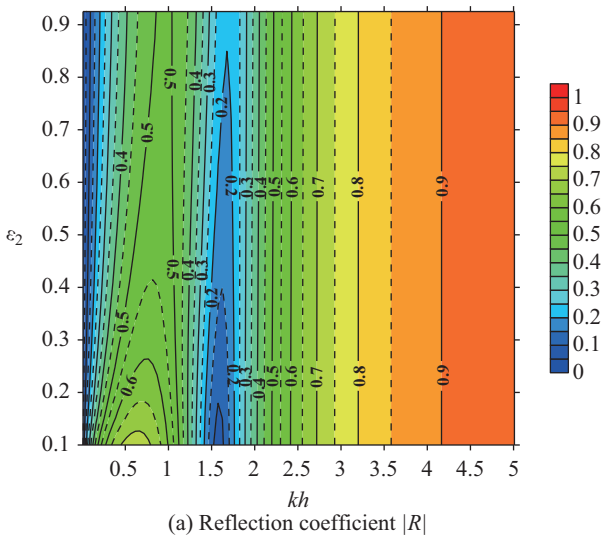

(a) Reflection coefficient $|R|$

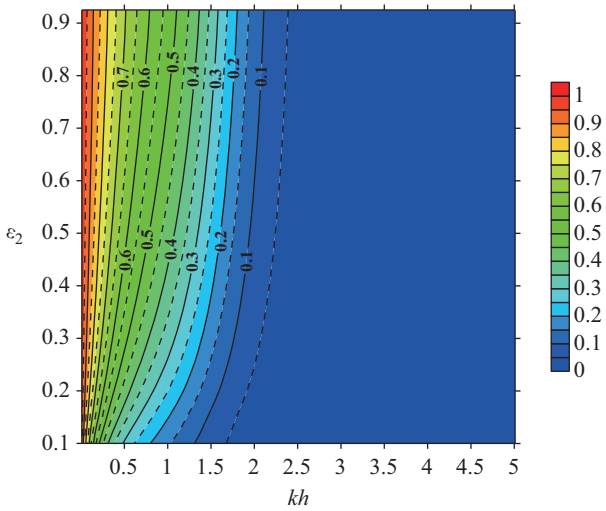

(b) Transmission coefficient $|T|$

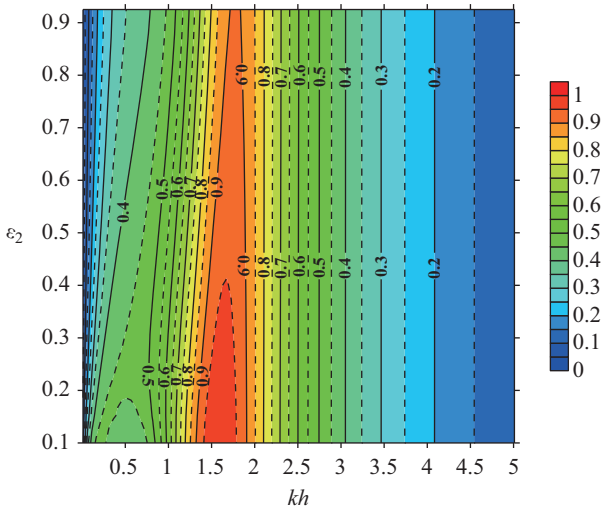

(c) Energy dissipation coefficient E_L

Fig. 8. Contour plots of $|R|$, $|T|$ and E_L coefficients as a function of kh and porosity ε_2 for double slotted walls at B/h = 0.5, ε_1 = 0.5, dm_1/h = 0.6, dm_2/h = 0.2.

dm_2/h), extensive calculations were conducted, and two contour plots are shown in Figs. 7 and 8. The friction factor (f) and the inertia coefficient (s) are taken as f = 2.0 and s = 1.0 throughout this comparison. In Figs. 7 and 8, a series of 2-D contour plots for various parameters are presented to demonstrate the optimal cases. Fig. 7 shows that the reflection and transmission coefficients are maintained at approximately 0.5 in a wide range of $1.0 < kh < 2.5$ when $dm_1/h = 0.6$ and $\varepsilon_1 = 0.5$. As observed in Fig. 7 (c), for the single vertical slotted wall breakwater at kh = 1.0~2.5, there exists an optimal porosity near $\varepsilon_1 = 0.5$ for the given fixed parameters. Next, we consider the performance of the double vertical slotted wall breakwater. More extensive calculations are conducted to plot $|R|$, $|T|$ and E_L coefficients as functions of both the non-dimensional wave number kh and porosity ε_2.

Fig. 8 shows that there is also an optimal porosity near $\varepsilon_2 = 0.3$ at $1.0 < kh < 2.5$ for the double vertical slotted walls breakwater with $dm_1/h = 0.6$, $\varepsilon_1 = 0.5$ and $dm_2/h = 0.2$. Using the two contour plots, we can find the smallest wave reflection and transmission and the largest wave energy dissipation for a particular combination of different porosities and different middle permeability parts. The wave reflection is not significantly reduced in the deep water waves (short waves) region at $kh > 3.0$.

4. Hydrodynamic Performance Comparison

Fig. 9 compares the hydrodynamic performance of the present model and the similar model investigated by Ahmed and Schlenkhoff (2014). The present numerical model assumes dm_1/h=0.6, dm_2/h=0.2, and B/h=0.5, where case (1) is $\varepsilon_1 = 0.5$ and $\varepsilon_2 = 0.3$ and case (2) is $\varepsilon_1 = \varepsilon_2 = 0.5$. The figures show that case (1) had a higher reflection coefficient, lower transmission and the highest energy dissipation coefficient. This can be attributed to the difference in the second vertical slotted walls with different permeable parts and porosity. In addition, the energy dissipation coefficient ranges between 0.8 and 0.963 when kh increase from 1.2 to 2.0, and the maximum value of the energy dissipation coefficient of 0.963 occurs at kh = 1.635.

IV. CONCLUSION

The multi-domain boundary element method (MBEM) was used to analyze the scattering of normal incident waves by double vertical slotted walls. The accuracy and validity of the method were verified through comparisons with results obtained by other authors using different methods. Based on the above numerical analysis and discussion, the following conclusions can be drawn: The multi-domain boundary element method (MBEM) adopted here is a simple, feasible, powerful and efficient scheme for the treatment of wave scattering problems, especially for solving problems involving a thin or non-thickness barrier. Numerical results have been presented for each type of double vertical slotted breakwater to show the effectiveness of the breakwater in reflecting incident waves, thus reducing the transmitted wave height. The reflection co-

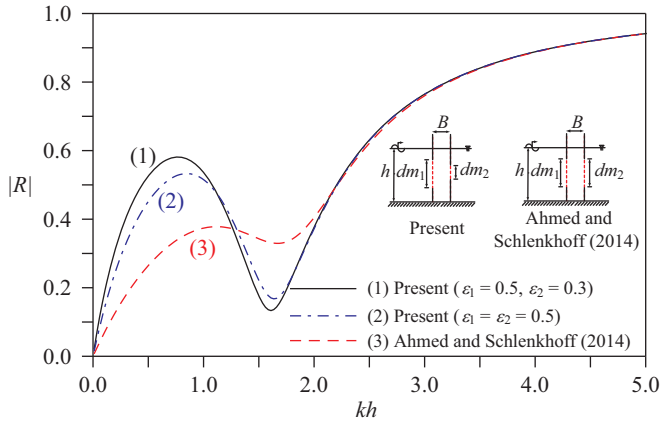

(a) Reflection coefficient $|R|$

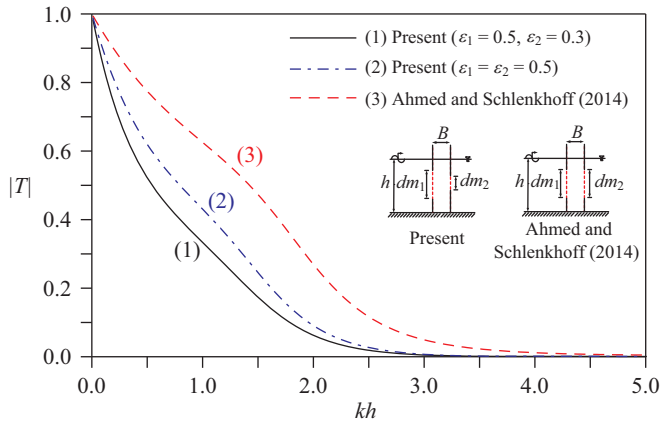

(b) Transmission coefficient $|T|$

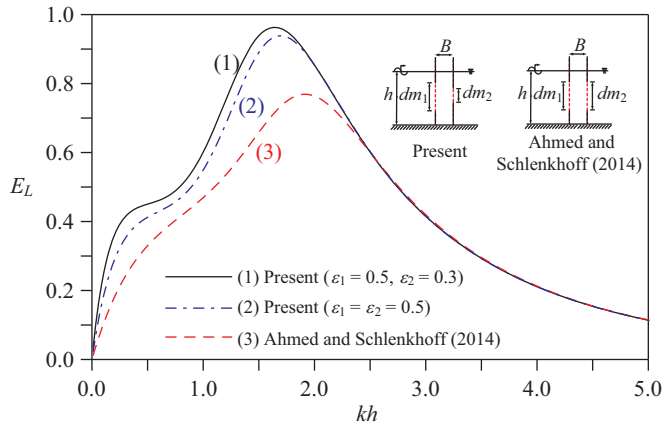

(c) Energy dissipation coefficient E_L

Fig. 9. Effect of the permeable middle part on the different porosities when $B/h = 0.5$ (1) $\varepsilon_1 = 0.5$, $\varepsilon_2 = 0.3$, $dm_1/h = 0.6$, and $dm_2/h = 0.2$; (2) $\varepsilon_1 = \varepsilon_2 = 0.5$, $dm_1/h = 0.6$, $dm_2/h = 0.2$; (3) $\varepsilon_1 = \varepsilon_2 = 0.5$, and $dm_1/h = dm_2/h = 0.6$.

efficient decreases as the permeable middle part of the seaward wall (dm_1/h) increases, and the transmission coefficient increases with increasing dm_1/h. Regardless of the variation in the relative chamber width, the maximum reflection coefficient occurs when the ratio of the chamber width (B) to the wavelength (L) is $B/L \approx 0.5$, which is associated with the minimum value of E_L. For double slotted walls, the chamber width should not be half the wavelength of the incident wave; the energy dissipation coefficient has a minimum at $B/L \approx 0.5$. In addition, our numerical results indicate that when the permeable middle part of the seaward (first) wall ($dm_1/h = 0.6$) and the permeable middle part of the leeward (second) wall ($dm_2/h = 0.2$) have porosities of $\varepsilon_1 = 0.5$ and $\varepsilon_2 = 0.3$, respectively, the breakwater has a high reflection coefficient, a low transmission coefficient and the maximum energy dissipation coefficient. The maximum energy dissipation coefficient of 0.963 occurs at $kh = 1.635$.

ACKNOWLEDGMENTS

The authors wish to express their gratitude for the financial aid from the Ministry of Science and Technology, Republic of China, and Project MOST No. 103-2221-E-019-065.

REFERENCES

Ahmed, H. and A. Schlenkhoff (2014). Numerical investigation of wave interaction with double vertical slotted walls. World Academy of Science, Engineering and Technology International Journal of Environmental, Ecological, Geological and Mining Engineering 8, 536-543.

Ahmed, H., A. Schlenkhoff, R. Rousta and R. Abdelaziz (2014). Experimental and semi-analytical investigation of wave interaction with double vertical slotted walls. International Science Index International Journal of Environmental, Ecological, Geological and Mining Engineering 8, 1435-1443.

Dean, W. R. (1945). On the reflexion of surface waves by a submerged plane barrier. Mathematical Proceedings of the Cambridge Philosophical Society 41, 231-238.

Isaacson, M., J. Baldwin, S. Premasiri and G. Yang (1999). Wave interactions with double slotted barriers. Applied Ocean Research 21, 81-91.

Isaacson, M., S. Premasiri and G. Yang (1998). Wave interactions with vertical slotted barrier. Journal of Waterway, Port, Coastal, and Ocean Engineering 124, 118-126.

Ji, C. H. and K. D. Suh (2010). Wave interactions with multiple-row curtainwall-pile breakwaters. Coastal Engineering 57, 500-512.

Koraim, A. S., M. M. Iskander and W. R. Elsayed (2014). Hydrodynamic performance of double rows of piles suspending horizontal c shaped bars. Coastal Engineering 84, 81-96.

Koraim, A. S. and T. N. Salem (2012). The hydrodynamic characteristics of a single suspended row of half pipes under regular waves. Ocean Engineering 50, 1-9.

Laju, K., V. Sundar and R. Sundaravadivelu (2007). Studies on Pile Supported Double Skirt Breakwater Models. The Journal of Ocean Technology 2, 32-53.

Laju, K., V. Sundar and R. Sundaravadivelu (2011). Hydrodynamic characteristics of pile supported skirt breakwater models. Applied Ocean Research 33, 12-22.

Liu, Y. and Y. C. Li (2010). The interaction of oblique waves with a partially immersed wave absorbing breakwater. In: Proceedings of the International Conference on Coastal Engineering no. 32, waves. 56.

Liu, Y. and Y. C. Li (2011). Wave interaction with a wave absorbing double curtain-wall breakwater. Ocean Engineering 38, 1237-1245.

Sollitt, C. K. and R. H. Cross (1972). Wave transmission through permeable breakwaters. Proceedings of 13th Conference on Coastal Engineering 3, 1827-1846.

Suh, K. D., S. Shin and D. T. Cox (2006). Hydrodynamic characteristics of pile-Supported vertical wall breakwaters. Journal of Waterway, Port, Coastal,

and Ocean Engineering 132, 83-96.
Sundar, V. and B. V. V. Subbarao (2002). Hydrodynamic pressure and forces on quadrant front face pile supported breakwater. Ocean Engineering 29, 193-214.
Sundar, V. and B. V. V. Subbarao (2003). Hydrodynamic performance characteristics of Quadrant front face Pile supported Breakwater. Journal of Waterway, Port, Coastal, and Ocean Engineering 129, 22-33.
Ursell, F. (1947). The effect of a fixed vertical barrier on surface waves in deep water. Mathematical Proceedings of the Cambridge Philosophical Society 43, 374-382.
Wiegel, R. L. (1960). A presentation of cnoidal wave theory for practical application. Journal of Fluid Mechanics 7, 273-286.
Yu, X. (1995). Diffraction of water waves by porous breakwaters. Journal of Waterway, Port, Coastal, and Ocean Engineering 121, 275-282.